Presented at the 33rd European PV Solar Energy Conference and Exhibition, 25-29 September 2017, Amsterdam, The Netherlands

A FAST AND EASY PEROVSKITE SOLAR CELL SIMULATION TOOL FEATURING ION MIGRATION

A. Fell[1], D. Walter[2], S. W. Glunz[1,3]

[1]Fraunhofer Institute for Solar Energy Systems, Freiburg, Germany
[2]The Australian National University, Canberra, Australia
[3]Department of Sustainable Systems Engineering (INATECH), Albert Ludwigs University Freiburg, Freiburg, Germany

ABSTRACT: Extensions for perovskite solar cells (PSCs) within the solar cell simulation tool Quokka3 are presented, accounting for ion migration. In the "1D detailed solver" the fully coupled equations describing semiconductor carrier transport, ion transport (anions and cations) as well as the general Shockley-Read-Hall formalism (trapping) are implemented, both as steady-state and transient mode. Numerical challenges arising from the narrowness of the Debye layer and the large difference in times scales between semiconductor and ion transport are successfully addressed. Example simulations are presented, showing the influence of pre-bias voltage on fast JV-sweeps, as well as an interaction between ion redistribution and surface recombination that replicates transient open-circuit voltage responses in a $MAPbI_3$ PSC.
Keywords: simulation, modelling, perovskite, ions, quokka

1 INTRODUCTION

Perovskite solar cells (PSCs) are one of the most promising candidates to replace, or via a tandem device enhance, the dominant Silicon photovoltaics (Si-PV) technology. Within several years only, record PSC R&D efficiencies are getting in the range of Si record efficiencies, clearly evidencing the performance potential. However, being a relatively young technology, the understanding of material properties and device physics is largely lacking behind the mature Si-PV technology. Reducing this gap is mandatory to succeed in developing long-term reliable PSCs for industrial application.

A key to gain understanding of PSCs is the ability to model its device physics. Besides significant uncertainties in material properties, one problem the community is facing is that PSCs exhibit a rather special combination of physical effects. In particular, it has been conclusively shown that both semiconductor current transport as well as ion migration play an important role to understand experimental observations and device performance [1–3]. This makes it not straight-forward to use established simulation tools from the semiconductor field and from other photovoltaic technologies, as they are not designed for such an application.

This paper presents the extension of Quokka3 to feature PSC-relevant models. Quokka is a popular "fast and easy" semiconductor simulation tool in the Si-PV community, and up to version 2 its focus was on multidimensional carrier transport in the quasi-neutral bulk [4]. However, Quokka3 features also a one-dimensional solver for the full semiconductor equations [5]. This "1D detailed solver" is where the PSC extensions, mainly ion migration, are included.

2 MODEL

2.1 Charge carrier transport equations

The model for describing carrier transport in the perovskite material is based on the well-established drift-diffusion model for semiconductor carrier transport (electrons and holes), extended by two additional charge carriers: anions and cations [7–9]. It is assumed that ions are neither generated nor "recombine", but a constant integral amount of ions solely redistributes within the perovskite material. Recombination of electrons and holes is considered via intrinsic mechanisms, i.e. Auger and radiative, as well as via the Shockley-Read-Hall (SRH) defect mechanism [6]. SRH can be modelled in its general or simplified form, the general form accounting for the effect of trapping on the charge density and resulting in unequal recombination rates for electrons and holes R_{el} and R_{hol}. The general system of 6 nonlinear differential equations to be solved then comprises the continuity equations for the 4 charge carrier densities

$$q\frac{dn}{dt} = q(G - R_{el}) - \frac{dJ_{el}}{dz}, \tag{1}$$

$$q\frac{dp}{dt} = q(G - R_{hol}) + \frac{dJ_{hol}}{dz}, \tag{2}$$

$$q\frac{dc_{an}}{dt} = -\frac{dJ_{an}}{dz}, \tag{3}$$

$$q\frac{dc_{cat}}{dt} = \frac{dJ_{cat}}{dz}, \tag{4}$$

the continuity equation for the trapped electron density

$$\frac{dn_t}{dt} = R_{el} - R_{hol}, \tag{5}$$

and the Poisson equation for the electric potential

$$\frac{d}{dz}\left(-\varepsilon\frac{d\varphi_e}{dz}\right) = q(N_D - N_A + p - n + c_{cat} - c_{an} - n_t). \tag{6}$$

The current densities due to drift and diffusion can be expressed via the quasi-Fermi potentials (i.e. the electrochemical potential) gradient, and the carrier concentration and mobility as

$$J_X = qc_X\mu_X\frac{d\phi_X}{dz}. \tag{7}$$

To solve those equations, one needs to relate the potentials to the carrier densities via carrier statistics. Fermi-Dirac statistics are applied for electrons and holes

$$n = N_c F_{1/2}\left(\frac{q\phi_{el} + E_c}{kT}\right), \tag{8}$$

$$p = N_v F_{1/2}\left(-\frac{q\phi_{hol} + E_v}{kT}\right), \tag{9}$$

and Boltzmann statistics for ions

$$c_{an} = N_{0,an}\exp\left(\frac{q(\phi_{an} + \varphi_e)}{kT}\right), \tag{10}$$

$$c_{cat} = N_{0,cat}\exp\left(-\frac{q(\phi_{an} + \varphi_e)}{kT}\right). \tag{11}$$

Optical modeling is outside the focus of this paper, and therefore the generation profile G is considered a user-input here.

2.2 Boundary conditions

At the time of writing this paper, Quokka3 supports two different kind of contact types forming the boundary conditions for semiconductor carrier transport: ideal contacts and metal-semiconductor (MS), i.e. Schottky, -type contacts. Both differentiate between an electron and hole contact, which determines the majority carrier type.

The ideal contact model pins the majority quasi-Fermi potential to the potential applied to the contact, and also assumes flat-band conditions, i.e. a zero electric field at the boundary.

The MS contact models majority carrier transport over the boundary via thermionic emission,

$$J_{maj} = A_0 T^2 \exp\left(-\frac{\Phi_B}{kT}\right)\left[\exp\left(\frac{\varphi_{cont}-\phi_{maj}}{kT/q}\right)-1\right] \pm J_{rec}, \quad (12)$$

and the electric potential is determined via

$$E_{c/v} = q\varphi_{cont} \pm \Phi_B. \quad (13)$$

The barrier-height Φ_B can either be directly defined by the user, or derived via the electron affinity of the perovskite material defining the band-edges E_c and E_v, and the (effective) work-function of the contact material

$$\Phi_B = \pm\left(E_{c/v} - WF\right). \quad (14)$$

Note that while fundamentally the contact potential is defined at the boundary, Quokka3 numerically allows the definition of a constant current as well. This is necessary to enable transient open-circuit simulations by setting the boundary current to zero.

Independently of the contact physics, surface recombination is modelled via the simplified SRH mechanism

$$J_{rec} = \frac{pn - n_{i,eff}^2}{S_{n0}(p_1+p)+S_{p0}(n_1+n)}. \quad (15)$$

Via this decoupling, in contrast to some other modeling tools where recombination and current transport over the boundary are essentially one and the same thing, complex contacts can be more easily approximated by their effective properties: effective barrier height and effective surface recombination properties.

As mentioned above, conservation of the integral ion concentration within the perovskite layer is assumed, meaning that the boundary conditions for ion transport is defined by zero current flow

$$J_{cat} = J_{an} = 0. \quad (16)$$

2.3 Implementation in Quokka3

The model detailed in the previous section is implemented within the "1D detailed solver" of Quokka3, using a finite-differences scheme. It supports solving the model both transient and steady-state, i.e. setting all time derivatives to zero. The steady-state solver is also used to find correct start values for the initial operating conditions of a transient simulation.

Despite this was observed to be numerically challenging in previous work [9], the numerical implementation allows a very fine mesh size towards the boundary, enabling the full numerical resolution of the Debye layer.

PSC modeling also benefits from the luminescence modeling implemented in Quokka3 [10]: from the electrical solution at any operating condition spectrally resolved luminescence is straightforward and numerically rapid to calculate from first principles, fully accounting for inhomogeneous carrier profiles and re-absorption effects. With this for example photoluminescence decay experiments accounting for ion migration can well be simulated.

Furthermore, Quokka3 implements two special features useful for modeling PSCs with ion migration: i) a pre-bias functionality of the steady-state solver, and ii) the option to set semiconductor transport to steady-state within the transient solver.

The pre-bias functionality allows the user to define a steady-state operating condition of the device which is solved including ion migration, before running the actual steady-state simulation with a "frozen" ion profile [11]. The primary application are fast JV-measurements after letting the PSC equilibrate at different conditions, as within the fast JV-sweep the slow-moving ions can well be assumed to have a constant distribution. This simplifies this type of simulations considerably, compared to trying to replicate the same within transient simulations.

Allowing to set semiconductor transport to steady-state within the transient solver, i.e. only solving ion-migration transiently, largely speeds up the simulation of the long time-scales required for the slow-moving ions. This is due to some unavoidable numerical inaccuracy resulting in considerable "noise" of the time derivatives of the, relatively, very fast electron and hole transport equations, which puts a limit on the maximum time step for successful convergence. This is resolved by only simulating the steady-state solution for each time step. Due to the large difference in time scales between semiconductor transport and ion migration, this quasi-steady-state approach is a highly valid assumption.

3 APPLICATION EXAMPLES

Two application examples showcasing the PSC functionality of Quokka3 are presented here. The common assumed device properties are listed in Table I. They represent typical values as reported in literature. It is noted however that uncertainties are large, and properties will vary for perovskite materials created by different processes. The exact values within those uncertainties are chosen such that the simulation results show the desired effects for illustrative examples.

Table I: (electrical) PSC device properties, mostly taken from [12].

property	symbol	value
band-gap	E_g	$1.5eV$
electron affinity	E_{EA}	$3.93eV$
relative permittivity	ε_r	30
electron mobility	μ_{el}	$2cm^2V^{-1}s^{-1}$
hole mobility	μ_{hol}	$2cm^2V^{-1}s^{-1}$
conduction band DOS	N_c	$2.2 \cdot 10^{18} cm^{-3}$
valence band DOS	N_v	$1.8 \cdot 10^{19} cm^{-3}$
net doping density	$N_D - N_A$	$0cm^{-3}$
defect density	N_t	$10^{15} cm^{-3}$
electron capture cross section	σ_n	$2 \cdot 10^{-14} cm^2$
hole capture cross section	σ_p	$2 \cdot 10^{-14} cm^2$
defect energy	$E_t - E_i$	0 (midgap)
front and rear electron SRV	S_{n0}	$10^5\ cm/s$
front and rear hole SRV	S_{p0}	$10^5\ cm/s$
hole contact work-function	WF	$5.3eV$
electron contact work-function	WF	$4.0eV$
average ion concentration	$N_{0,an/cat}$	$5 \cdot 10^{18} cm^{-3}$
anion mobility	μ_{an}	0 (immobile)
cation mobility	μ_{cat}	$2 \cdot 10^{-12} cm^2V^{-1}s^{-1}$
uniform generation rate	G	$3 \cdot 10^{21} cm^{-3}$
device thickness	W	$400nm$

3.1 Pre-bias impact on JV-curves

In this example, the pre-bias functionality is showcased. A steady-state solution for the PSC at different bias voltages is simulated, and subsequently a steady-state light JV-curve is simulated with immobile ions. This represents a fast JV-sweep after the different pre-bias conditions, for which redistribution of the slow-moving ions is negligible, an approach often used to characterize PSCs experimentally [9,11].

Figure 1 shows the resulting light JV-curves for pre-bias voltages ranging from 0V to 1.2V. The expected trends from reported experiments can clearly be seen, which are caused by the different ion distributions shown in Figure 2.

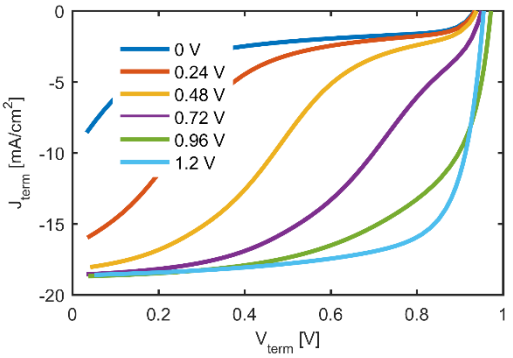

Figure 1: Simulated JV-curves for different immobile cation concentration profiles resulting from different pre-bias voltage steady-state simulations with mobile cations, representing rapid JV-sweeps after different pre-bias conditions.

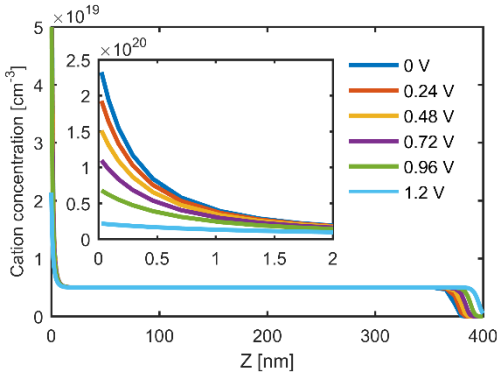

Figure 2: Steady-state cation concentration profiles for the different pre-bias voltages, showing the full numerical resolution of the narrow Debye layer.

3.2 Transient open-circuit voltage during ion relaxation

In the example shown in Figure 3, the influence of transient ion redistribution on the relaxation of open circuit voltage is demonstrated, in comparison to experimental data. A known example of hysteresis in $MAPbI_3$ PSCs is a transient, non-monotonic "overshoot" of the open-circuit voltage when a PSC is abruptly illuminated under open-circuit conditions [1,11]. The cell is initially at steady-state in the dark and then illuminated at t = 0s. In response to the generation of electron-hole pairs, the electric field in the device changes, causing the dark steady-state ion concentration to redistribute towards the illuminated open-circuit steady-state condition. As it does so, the measured voltage is affected by changing recombination currents in the bulk and at the cell surface. With the addition of only a single mobile cation population on top of the standard drift-diffusion model, one of the more counter-intuitive experimental measurements can be qualitatively replicated. Furthermore, the log of the simulated PL signal is plotted, which is approximately proportional to the internal Fermi-Level split or implied V_{OC}. For the case of high surface recombination, it shows a different trend to the (external) V_{OC}, caused by a majority carrier potential drop close to the surfaces which varies over time.

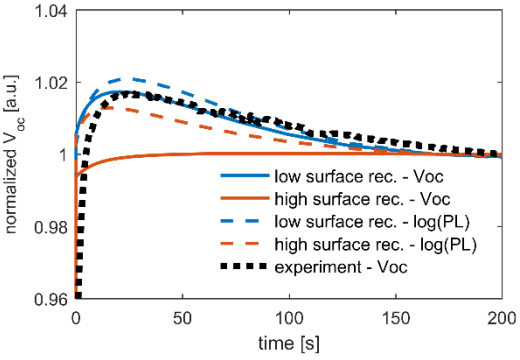

Figure 3: Measurement of V_{oc} transient in response to illumination in $MAPbI_3$ PSC (dashed line), compared to simulated responses with mobile cations. Both the (external) V_{OC} and the log of the PL signal is simulated, showing a different trend for high surface recombination.

4 CONCLUSIONS

Several extensions to the 1D detailed solver within Quokka3 allow the consideration of important effects particular to PSCs, mainly ion migration. A numerical solver for the fully coupled semiconductor and ion drift-diffusion equations is successfully implemented, both for the steady-state and transient case. The solver can account for the effect of trapping within the perovskite material, by implementing the general SRH formalism. The luminescence modelling implemented in Quokka3 further allows for an accurate prediction of spectrally resolved luminescence signal, accounting for non-uniform carrier profile and re-absorption effects.

Two special features of Quokka3 useful for PSC simulations are highlighted by application examples: i) a pre-bias functionality, allowing (fast) steady-state simulations with a fixed ion distribution calculated at a steady-state pre-bias point, useful in particular for representing fast JV-sweeps after different pre-bias conditions; ii) an option to solve semiconductor transport as (quasi-)steady-state within the transient solver, removing numerical limitations due to the large differences in times scales between semiconductor and ion transport.

Currently only the perovskite material layer is solved. Electron and hole contact layers are not resolved but modelled via an effective work-function and surface recombination boundary condition. However, given the large uncertainties and number of unknowns within the perovskite material, resolving the physics within the electron and hole contact materials can be considered a second-order effect.

Nonetheless, work towards implementing multiple semiconductor material layers and interface physics is currently under way, including also (effective) tunneling interfaces. By treating the top-cell as quasi-1D within the skin-concept of Quokka3, this will enable 2D / 3D simulation of tandem cells resolving an unprecedented amount of physical effects.

ACKNOWLEDGEMENTS

Andreas Fell acknowledges funding by the European Commission through the Marie-Curie fellowship “Quokka maturation”.

REFERENCES

[1] W. Tress, N. Marinova, T. Moehl, S.M. Zakeeruddin, M.K. Nazeeruddin, M. Grätzel, Understanding the rate-dependent J–V hysteresis, slow time component, and aging in CH 3 NH 3 PbI 3 perovskite solar cells: the role of a compensated electric field, Energy & Environmental Science 8 (3) (2015) 995–1004.

[2] C. Eames, J.M. Frost, P.R.F. Barnes, B.C. O’regan, A. Walsh, M.S. Islam, Ionic transport in hybrid lead iodide perovskite solar cells, Nature communications 6 (2015) 7497.

[3] H.J. Snaith, A. Abate, J.M. Ball, G.E. Eperon, T. Leijtens, N.K. Noel, S.D. Stranks, J.T.-W. Wang, K. Wojciechowski, W. Zhang, Anomalous hysteresis in perovskite solar cells, The journal of physical chemistry letters 5 (9) (2014) 1511–1515.

[4] A. Fell, A Free and Fast Three-Dimensional/Two-Dimensional Solar Cell Simulator Featuring Conductive Boundary and Quasi-Neutrality Approximations, IEEE Transactions on Electron Devices 60 (2) (2013) 733–738.

[5] A. Fell, J. Schön, M.C. Schubert, S.W. Glunz, The concept of skins for silicon solar cell modeling, Solar Energy Materials and Solar Cells (2017).

[6] W. Shockley, W.T. Read Jr, Statistics of the recombinations of holes and electrons, Physical Review 87 (5) (1952) 835.

[7] P. Calado, A.M. Telford, D. Bryant, X. Li, J. Nelson, B.C. O’regan, P.R.F. Barnes, Evidence for ion migration in hybrid perovskite solar cells with minimal hysteresis, Nature communications 7 (2016) 13831.

[8] S. van Reenen, M. Kemerink, H.J. Snaith, Modeling anomalous hysteresis in perovskite solar cells, The journal of physical chemistry letters 6 (19) (2015) 3808–3814.

[9] G. Richardson, S.E.J. O'Kane, R.G. Niemann, T.A. Peltola, J.M. Foster, P.J. Cameron, A.B. Walker, Can slow-moving ions explain hysteresis in the current–voltage curves of perovskite solar cells?, Energy & Environmental Science 9 (4) (2016) 1476–1485.

[10] A. Fell, K.R. McIntosh, M. Abbott, D. Walter, Quokka version 2: selective surface doping, luminescence modeling and data fitting, in: 23rd Photovoltaic Science and Engineering Conference (PVSEC), Taipei, 2013.

[11] D.A. Jacobs, Y. Wu, H. Shen, C. Barugkin, F.J. Beck, T.P. White, K. Weber, K.R. Catchpole, Hysteresis phenomena in perovskite solar cells: The many and varied effects of ionic accumulation, Physical Chemistry Chemical Physics 19 (4) (2017) 3094–3103.

[12] Y. Wu, H. Shen, D. Walter, D. Jacobs, T. Duong, J. Peng, L. Jiang, Y.-B. Cheng, K. Weber, On the Origin of Hysteresis in Perovskite Solar Cells, Advanced Functional Materials 26 (37) (2016) 6807–6813.